**Congshan Li**[*]**,**
**Xiaowei Zhang,**
**Yan Liu,**
**Ping He,**
**Pu Zhong,**
**Yan Fang**

**Regular paper**

# Analysis on damping characteristics of multi-terminal VSC-HVDC system connected to wind farm

In order to study the influence of wind power grid connection on the small-signal stability of the multi-terminal VSC-HVDC system, based on the complete doubly-fed wind turbine model, damping characteristics of the multi-terminal VSC-HVDC system are qualitatively analyzed. Analyzed the influence of the doubly-fed induction generator (DFIG)-based wind turbine (WT) connection on the damping characteristics and stability of the multi-terminal VSC-HVDC system from multiple perspectives including the access point of the WT, the WT's capacity and transmission distance. The methods of the eigenvalue analysis and time-domain simulation analysis are adopted in this paper. Firstly, a complete three-terminal VSC-HVDC system model is built in PSCAD, and the systems after the WT connected to the grid are analyzed and compared. Then, based on the total least squares-estimation of signal parameters via rotational invariance techniques (TLS-ESPRIT) algorithm, some information of the system can be obtained such as eigenvalue, frequency, damping ratio and so on. The research results show that when the WT is connected to the inverter side, the damping ratio tends to be greater than connected to the rectifier side. In addition, within a certain range, as the capacity and transmission distance of the WT increase, the damping ratio also tends to increase. In this way, it provides a technical reference for the planning of wind farm access to multi-terminal VSC-HVDC system.

Keywords: Damping characteristic; multi-terminal VSC-HVDC system; low frequency oscillation; wind farm

## 1. Introduction

With the advancement of power electronics technology, VSC-HVDC system as a new generation of direct current (DC) transmission technology, can easily solve many problems faced by current AC and DC transmission technology, and provide a new solution for the transformation of power transmission methods and the construction of future power grids [1]. Since the super grid plan is proposed in Europe in 2008 [2], the world's first multi-terminal VSC-HVDC transmission demonstration project has been built on Nan'ao Island [3], the world's first five-terminal VSC-HVDC transmission project has also been put into operation in Zhoushan Island in China [4]. In addition, Zhangbei demonstration project which is the world's first demonstration of VSC-HVDC loop grid has been officially put into operation [5]. Thus, VSC-HVDC transmission system has entered a stage of rapid development. At the same time, as a new energy with advantages in alleviating energy crisis, protecting the environment, promoting energy and environmental sustain-able development, wind energy is highly valued by countries all over the world [6-8].

As wind power generation technology gradually matures, it is gradually integrated into the VSC-HVDC transmission system on a large scale. At the same time, it also brings new challenges such as the various oscillations in the VSC-HVDC system. Studies have shown that the stability problems caused by the connection of large-capacity wind turbines to the

[*] Corresponding author: Department of Electrical and Information Engineering, Zhengzhou University of Light Industry, Zhengzhou, Henan, 450002, PRC, E-mail: 543627767@qq.com
Department of Electrical and Information Engineering, Zhengzhou University of Light Industry, Zhengzhou, 450002 P.R. China

VSC-HVDC system can't be ignored [9-12]. Thus, various oscillation problems caused by the system have become an important research direction.

At present, the feeding of new energy into the multi-terminal DC system has become one of the future development trends, so when the WT is integrated into the multi-terminal HVDC system, the stability of the system is worth analyzing and studying. References [9-10] and references [11-12] pointed out that the interaction between the control systems of wind farm and HVDC station will cause the stability problem of the interconnected system, which mainly is based on the methods of sequence impedance analysis and the characteristic root analysis. Reference [13] studied the interconnection system of wind farms and modular multilevel converter based high voltage DC transmission (MMC-HVDC) used the characteristic root method, and the study showed that as the output of wind farms increases, the interconnected system will experience oscillation instability. References [14-15] studied the sub-synchronous damping characteristics of the alternating current (AC)/DC hybrid system with conventional DC transmission system, and the research showed that improper setting of the relevant parameters of the converter will bring about the risk of sub-synchronous oscillation. Reference [16] uses the small signal analysis method to study the HVDC system with DFIG, and analyzes the damping through characteristic roots, but does not explain the mechanism of oscillation. Reference [17] established an impedance model based on direct-drive WT, analyzing the cause of oscillation, and believed that its port exhibits capacitive negative resistance characteristics within a specific frequency range, which causes sub-synchronous oscillations with the inductive AC power grid. In addition, reference [18] studied the causes of sub-synchronous oscillations in the system from the perspective of electromagnetic torque, and studied the influence of the parameters of the HVDC system controller and the steady-state transmission power on the system stability.

Under the above background, this paper studies the influence of the connection of the DFIG-based WT into multi-terminal VSC-HVDC system on the low-frequency oscillation mode and damping characteristics from multiple aspects such as the WT's location, capacity and transmission distance. This paper adopts the methods of eigenvalue analysis and time-domain simulation analysis. Firstly, the three-terminal VSC-HVDC system model of wind power grid-connected is established on the PSCAD/EMTDC simulation platform, and the corresponding power angle curve is obtained by simulation. Then, the TLS-ESPRIT algorithm is used to identify the eigenvalues of the system and other information. Based on this, the influence of the access point, capacity, and transmission distance of the WT on the system oscillation and damping characteristics is obtained. Considering this, the research can provide corresponding technical reference for the planning of wind power grid connection to multi-terminal VSC-HVDC system.

## 2. Model analysis and Low frequency oscillation research method

### 2.1. DFIG-based WT model

Wind power generation systems differ according to the generator operation mode, which can be divided into constant speed and constant frequency wind power generation systems and variable speed and constant frequency wind power generation systems [19]. Because the DFIG has the advantages of small excitation inverter capacity, low cost, and variable-speed constant-frequency operation, the application of doubly-fed power generation systems is extensive and the research is getting deeper and deeper [20].

### 2.1.1. System structure of DFIG-based WT model

DFIG-based WT is mainly composed of a wind turbine system and a doubly-fed power generation system. The wind turbine system can capture wind energy and realize power control, and convert wind energy into mechanical energy. At the same time, the double-fed power generation system can realize the conversion of mechanical energy to electric energy [21], and the structure of the DFIG-based WT system is shown in Fig. (1).
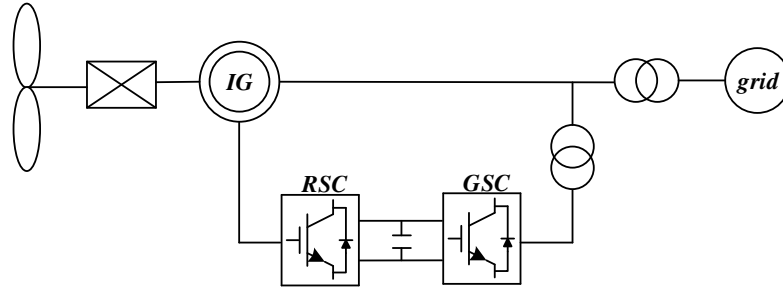


Fig.1. The DFIG-based WT model

2.1.2. Mathematical model of DFIG-based WT

DFIG-based WT has the characteristics of high-order and strong coupling, and its operating characteristics are very complex. Apply park transformation to transform the basic electromagnetic relationship of the doubly-fed induction generator on the *abc* axis of the coordinate system to the $d$-$q$ axis coordinate system of the rotor [22]. Then, the voltage equation, flux equation, power equation and torque equation on the $d$-$q$ axis of the coordinate system can be obtained.

The expression of the DFIG-based wind turbines' voltage is:

$$u_{ds} = -R_S i_{ds} + \frac{d\psi_{ds}}{dt} - \omega\psi_{qs} \tag{1}$$

$$u_{qs} = -R_S i_{qs} + \frac{d\psi_{qs}}{dt} + \omega\psi_{ds} \tag{2}$$

$$u_{dr} = R_r i_{dr} + \frac{d\psi_{dr}}{dt} - \omega_s\psi_{qr} \tag{3}$$

$$u_{qr} = R_r i_{qr} + \frac{d\psi_{qr}}{dt} + \omega_s\psi_{dr} \tag{4}$$

Where $u_{ds}$, $u_{dr}$ are the stator voltage and the rotor voltage of $d$−axis, $u_{qs}$, $u_{qr}$ are the stator voltage and the rotor voltage of $q$−axis, $i_{ds}$, $i_{dr}$ are the stator current and the rotor current of $d$−axis, $i_{qs}$, $i_{qr}$ are the stator current and the rotor current of $q$−axis, $R_s$, $R_r$ are the resistance of stator and rotor, $w$ represents the synchronous speed, $w_s$ represents the slip speed.

The flux linkage equation is

$$\psi_{ds} = -L_{ss}i_{ds} + L_m i_{dr} \tag{5}$$
$$\psi_{qs} = -L_{ss}i_{qs} + L_m i_{qr} \tag{6}$$
$$\psi_{dr} = L_{rr}i_{dr} - L_m i_{ds} \tag{7}$$
$$\psi_{qr} = L_{rr}i_{qr} - L_m i_{qs} \tag{8}$$

Where $\varphi_{ds}$, $\varphi_{dr}$ are stator flux linkage and the rotor flux linkage of $d-$ axis, $\varphi_{qs}$, $\varphi_{qr}$ are stator flux linkage and the rotor flux linkage of $q-$ axis, $L_s$, $L_r$ are respectively inductance

of the stator and rotor, $L_m$ represents mutual inductance. In addition, $L_{ss} = L_s + L_m$, $L_{rr} = L_r + L_m$.

The DFIG-based WT's active power output equation is

$$P_s = u_{ds}i_{ds} + u_{qs}i_{qs} \tag{9}$$

$$P_r = u_{dr}i_{dr} + u_{qr}i_{qr} \tag{10}$$

$$P_g = u_{dg}i_{dg} + u_{qg}i_{qg} \tag{11}$$

$$P_{DFIG} = P_s + P_g \tag{12}$$

Where $P_s$, $P_r$, $P_g$ are the active power output of the stator-side, rotor-side and grid-side converters respectively, $P_{DFIG}$ is the active power output of the DFIG-based WT.

The DFIG-based WT's reactive power output equation is

$$Q_s = u_{qs}i_{ds} - u_{ds}i_{qs} \tag{13}$$

$$Q_g = u_{qg}i_{dg} - u_{dg}i_{qg} \tag{14}$$

$$Q_{DFIG} = Q_s + Q_g \tag{15}$$

Where $Q_s$ and $Q_g$ are the reactive power output of the rotor-side converter and the grid-side converter, $Q_{DFIG}$ is the reactive power output of the DFIG-based WT. In addition, usually $Q_g = 0$.

The rotor-side's electromagnetic power output equation is

$$Pes = L''(\psi_{ds}i_{qr} - \psi_{qs}i_{dr}) \tag{16}$$

The DFIG-based WT's electromagnetic torque output equation is as follows

$$T_e = \frac{P_{DFIG}}{W_r} = \frac{(1-s)P_{es}}{(1-s)w} = P_{es} = L''(\psi_{ds}i_{qr} - \psi_{qs}i_{dr}) \tag{17}$$

2.2. System model

2.2.1. Multi-terminal VSC-HVDC system model

The multi-terminal VSC-HVDC system is a DC system containing three or even more voltage source converter stations. Unlike the double-ended DC transmission system which has only one DC transmission line, the multi-terminal VSC-HVDC system requires multiple DC transmission lines. According to different operating conditions and design requirements, the multi-terminal VSC-HVDC power trans-mission system mainly has three connection modes: series, parallel and hybrid. What this text establishes is radiating three-terminal VSC-HVDC interconnection system in parallel as shown in Fig. (**2**). In addition, the converter stations in the multi-terminal VSC-HVDC system adopt constant active power control.
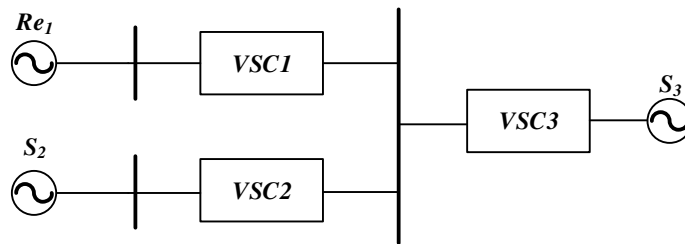


Fig. 2. Three-terminal VSC-HVDC system

In the fig. (**2**), $Re_1$ is a voltage source with rated capacities of 100 MW. $S_2$ and $S_3$ are generator systems where rated capacities both are 360 MW. In addition, VSC1 and VSC2 are rectifier stations, and VSC3 is an inverter station where rated capacity is 60 MW, 60 MW and 120 MW respectively. At the same time, when the active power of the converter station is injected into the AC side, the direction is assumed to be positive.

2.2.2. Multi-terminal VSC-HVDC system model with DFIG-based WT

In order to analyze the impact of wind power on the multi-terminal VSC-HVDC grid, this paper uses an interconnection system composed of the DFIG-based WT and three-terminal VSC-HVDC system which can be seen as follows. In Fig. (**3**), ① and ② indicate that the DFIG-based WT is connected in parallel on the rectifier side and the inverter side of multi-terminal VSC-HVDC system respectively.
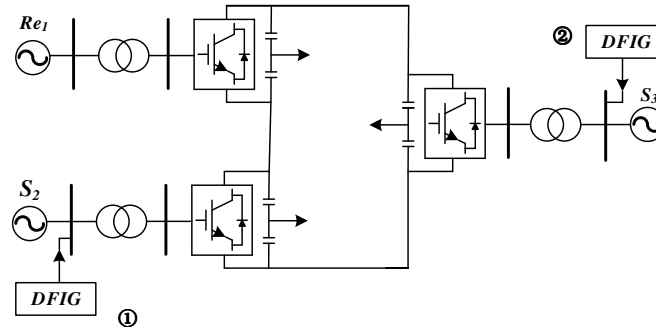


Fig. 3. The DFIG-based WT and three-terminal VSC-HVDC connected to the Grid

2.3. Low frequency oscillation research method

There have been many mature research methods for the analysis of low-frequency oscillation characteristics in power systems, including methods based on modal, measurement signal and low-frequency oscillation characteristics analysis built on probabilistic small disturbance stability [18]. At the same time, the signal analysis method based on the measured signal is a hot spot in the current research on low-frequency oscillation of the power system. System identification is an important branch of signal analysis method, which can be used to obtain system oscillation mode parameters. System identification includes a variety of identification algorithms. This paper uses the TLS-ESPRIT algorithm which has a stronger robustness to identify low-frequency oscillation modes.

2.3.1. Basic principles of TLS-ESPRIT algorithm identi-fication

The TLS-ESPRIT identification algorithm is a high-resolution signal analysis method formed on the signal subspace, which is evolved from the ESPRIT algorithm [23]. The principle of ESPRIT is to calculate the rotation factor of the signal by sampling the data, and to improve the reliability and robustness of the ESPRIT algorithm by adding TLS. The mathematical principles of the TLS-ESPRIT algorithm are as follows.

(1) First, sample the low-frequency oscillation signal, and then sort the sampled low-frequency oscillation signal into a combination of attenuated sinusoidal signal and white noise. The mathematical formula for the low-frequency oscillation signal at sampling time $n$ is as follows:

$$x(n) = \sum_{k=1}^{p} \alpha_k e^{j\theta_k} e^{j(-\sigma_k + jw_k)nT_s} + w(n) \tag{18}$$

Where $P$, $T_s$, $w(n)$ are the mode order, sampling period and white Gaussian noise of the system. $\alpha_k$, $\theta_k$, $\sigma_k$ are respectively the amplitude of the $k-th$ attenuated sine, the initial phase, the attenuation coefficient and angular frequency.

(2) Construct a Hankel matrix $X$ for the sampled original sequence $X(n)$ shown as follows.

$$X = \begin{bmatrix} x(0) & x(1) & \cdots & x(M-1) \\ x(1) & x(2) & \cdots & x(M) \\ \vdots & \vdots & \ddots & \vdots \\ x(L-1) & x(N-L) & \cdots & x(N-1) \end{bmatrix} \tag{19}$$

Where $L$ is the number of data records or snapshots, $M$ is the length of the time. In addition, $L, M > P$, $L+M-1=N$.

(3) Perform singular value decomposition of $X$ to obtain signal subspace and noise subspace shown as follows.

$$X = U \Lambda V^H = \begin{bmatrix} U_S & U_N \end{bmatrix} \begin{bmatrix} \sum_S & 0 \\ 0 & \sum_N \end{bmatrix} \begin{bmatrix} V_S^H \\ V_N^H \end{bmatrix} \tag{20}$$

Where $U$ and $V$ are classified according to the singular value of the signal space, the subscripts $S$ and $N$ are respectively the signal subspace and the noise subspace, the superscript $H$ is the conjugate transpose, $\Lambda$ represents the diagonal matrix, $U$, $V$ Corresponding to the unitary matrix of $L \times L$ and $M \times M$ respectively.

(4) The signal subspace after singular value decomposition has rotation invariance. So the signal subspace can be divided into two interwoven subspaces. In addition, the reversible diagonal matrix $\psi$ can be found so that the following formula holds.

$$V_S = \begin{bmatrix} V_1 \\ \cdots \end{bmatrix} = \begin{bmatrix} \cdots \\ V_2 \end{bmatrix} \tag{21}$$

$$V_2 = V_1 \psi$$

Where $V_1$, $V_2$ are respectively the matrixes obtained by removing the last row and the first row of matrix $S_v$. Then, the matrix $V$ is constructed through matrix $V_1$ and matrix $V_2$, and the singular value decomposition of $V$ is performed to obtain the matrix $V_t$ shown as follows.

$$V = \begin{bmatrix} V_1 & V_2 \end{bmatrix}$$

$$V_t = \begin{bmatrix} V_{11} & V_{12} \\ V_{21} & V_{22} \end{bmatrix} \tag{22}$$

(5) By obtaining the eigenvalue $\lambda_k$ of the matrix $\psi_{TLS}$ ( $k=1,2,3\cdots p$ ), some information can be estimated such as the frequency $f_k$, damping factor $\sigma_k$ and damping ratio $\xi_k$ of the signal as follows.

$$f_k = \frac{\arctan(\frac{\mathrm{Im}(\lambda_k)}{\mathrm{Re}(\lambda_k)})}{2\pi T_s}$$

$$\sigma_k = -\frac{\mathrm{I}n|\lambda_k|}{T_s} \tag{23}$$

$$\xi_k = \frac{-\sigma_k}{\sqrt{\sigma^2 + (2\pi f_k)^2}}$$

(6) Then use the method of the least square to get the amplitude and the initial phase angle. In addition, according to the sampling signal at $N$ point, the formula can be obtained as follows.

$$H = \lambda_0 \times Y \tag{24}$$

Next, by using the least square method again, the solution of the above formula can be obtained as follows.

$$Y = (\lambda_b{}^H \lambda_b)^{-1} \lambda_b{}^H H \tag{25}$$

At last, the amplitude and the initial phase can be calculated as follows.

$$\sigma_k = 2|Y_k|$$

$$\theta_k = \arctan(\frac{\mathrm{Im}(Y_k)}{\mathrm{Re}(Y_k)}) \tag{26}$$

## 3. Simulation and analysis results

The WT in the simulation model is a DFIG-based WT where rated power is 100MVA and rated output voltage is 13.8kV. In addition, the specific parameters of the model are shown in Table 1.

Table 1: Model parameters

| Parameter | Value |
|---|---|
| Generator rated power/MVA | 100 |
| Generator rated voltage /kV | 13.8 |
| Frequency/rad.s-1 | 376.99 |
| Stator-rotor turns ratio | 3 |
| Moment of inertia/s | 0.7267 |
| Mechanical damping(pu) | 0.001 |

3.1. Impact of WT's location on the damping characteri-stics of the system

The wind speed of the DFIG-based WT is set to 11.5m/s during the initial operation. After 8s, the wind speed becomes 10.5m/s. First, the WT is incorporated at ① in Fig. (**3**) where a set of time-domain data is obtained by simulation. Then apply a small disturbance excitation signal to the system. The specific implementation method is to decrease the power command value by 0.02 at two seconds at the converter station 1, and obtain another set of time domain data through simulation. Thus, the two sets of generator power angle

data before and after the disturbance are obtained. At last, the two sets of sampled data are analyzed through the TLS-ESPRIT algorithm to obtain the identified oscillation modes which is shown in Table 2 as follows.

Table 2: Oscillation model identification results

| Oscillation Mode | Eigenvalue | Frequency/Hz | Damping ratio/% |
| --- | --- | --- | --- |
| LFO mode 1 | -0.0443+1.7081i | 0.2719 | 2.59 |
| LFO mode 2 | -0.0214+ 2.5344i | 0.4034 | 0.84 |
| LFO mode 3 | -0.0336+ 5.5329i | 0.8806 | 0.61 |

It can be seen from Table 2 that there are three oscillation modes, all of which are low frequency oscillation (LFO) modes, and their damping ratios gradually decrease with increasing frequency. In addition, the damping ratios of the three modes are relatively small.

Use the same method to obtain the two sets of generator power angle data when the WTs are connected in parallel at ② in Fig. **3**. Then, the two sets of data sampled are analyzed through the TLS-ESPRIT algorithm to obtain the identified oscillation modes which is shown in Table 3 as follows.

Table 3: Oscillation model identification results

| Oscillation Mode | Eigenvalue | Frequency/Hz | Damping ratio/% |
| --- | --- | --- | --- |
| LFO mode 1 | -0.0838+ 4.2696i | 0.6795 | 1.96 |
| LFO mode 2 | -0.0761+ 7.1505i | 1.1380 | 1.06 |
| LFO mode 3 | -0.0927+ 9.0946i | 1.4474 | 1.02 |

It can be seen from Table 3 that the system also has three low-frequency oscillation modes. As the frequency increases, the corresponding damping ratio gradually decreases, and the damping ratios of these modes are relatively weak.
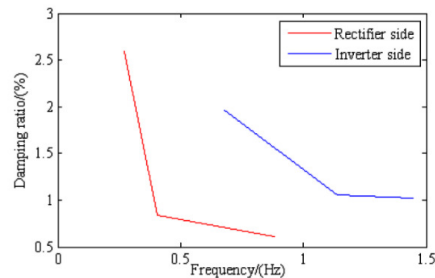


Fig. 4. Different access point of DFIG-based WT

As can be seen from the frequency-damping ratio characteristic in Fig. (**4**), when the WT is connected to the multi-terminal VSC-HVDC from the rectifier side, the damping ratio

shows a downward trend with the increase of frequency, all showing a low frequency oscillation mode. When the WT is connected to the multi-terminal VSC-HVDC system from the inverter side, the damping ratio also shows a downward trend as the frequency increases. At the same time, it can be seen from the two sets of curves that at the same oscillation frequency, the damping ratio of the WT integrated into the inverter side is greater than that of the WT integrated into the rectifier side.

3.2. Impact of WT's capacity on the damping characteri-stics of the system

By changing the capacity of the WT, the influence of WT on the oscillation mode and damping characteristics of the multi-terminal VSC-HVDC system is analyzed. Corresponding simulations are made where the capacity of the WT in different locations is changed. First, the WT's capacity is increased from 100MW to 150MW. Then, the TLS-ESPRIT algorithm is used to analyze the sampled two sets of generator power angle data to obtain the identified oscillation modes.

Table 4: Oscillation model identification results

| Oscillation Mode | Eigenvalue | Frequency/Hz | Damping ratio/% |
|---|---|---|---|
| LFO mode 1 | -0.0457±1.1812i | 0.1880 | 3.86 |
| LFO mode 2 | -0.0663±2.2770i | 0.3624 | 2.91 |
| LFO mode 3 | -0.0243±5.3594i | 0.8530 | 0.45 |

Table 4 shows the differences caused by change of WT's capacity in the system oscillation mode and damping characteristic when the WT's position is at ① of Fig. (**3**). As we can see from Table 4 that there are three low-frequency oscillation modes. Also, the damping ratio gradually decreases to almost zero as the frequency increases.
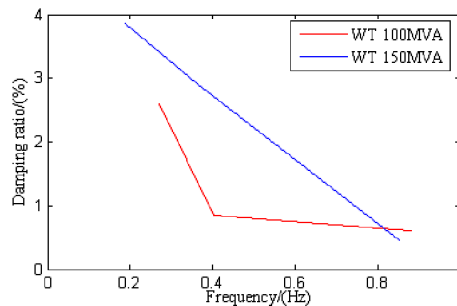


Fig. 5. Different capacity of DFIG-based WT in the rectifier side

As can be seen from the frequency-damping ratio characteristic of Fig. (**5**), when the WT is located in the rectifier side of the multi-terminal VSC-HVDC system, at the same oscillation frequency, the larger the wind turbine capacity is, the bigger the damping ratio is.

Table 5: Oscillation model identification results

| Oscillation Mode | Eigenvalue | Frequency/Hz | Damping ratio/% |
|---|---|---|---|
| LFO mode 1 | -0.2559±5.3651i | 0.8539 | 4.76 |
| LFO mode 2 | -0.1432±8.4157i | 1.3394 | 1.70 |
| LFO mode 3 | -0.1149±9.7229i | 1.5474 | 1.18 |

Table 5 shows the differences caused by change of WT's capacity in the system oscillation mode and damping characteristic when the WT's position is at ② of Fig (**3**). As we can see from Table 5 that there are three low-frequency oscillation modes. Also, the damping ratio gradually decreases as the frequency increases.
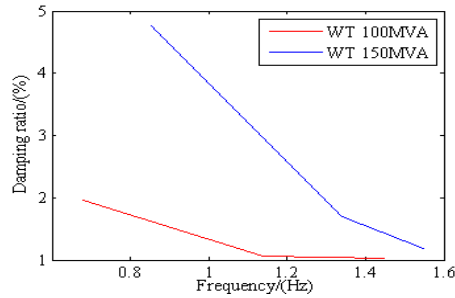


Fig. 6. Different capacity of DFIG-based WT in the inverter side

As can be seen from the frequency-damping ratio characteristic of Fig. (**6**), when the WT is located in the inverter side of the multi-terminal VSC-HVDC system, at the same oscillation frequency, the larger WT's capacity is, the larger the corresponding damping ratio tends to be.

3.3. Impact of WT's transmission distance on the damping characteristics of the system

By changing the WT's transmission distance, the influence of WT on the oscillation mode and damping characteristics of the multi-terminal VSC-HVDC system is analyzed. Corresponding simulations are made where the WT's transmission distance in different locations is changed. First, transmission distance of the WT where its capacity is 150 MW is decreased from 4000km to 3000km. Then, the TLS-ESPRIT algorithm is used to analyze the sampled two sets of generator power angle data to obtain the identified oscillation modes.

Table 6: Oscillation model identification results

| Oscillation Mode | Eigenvalue | Frequency/Hz | Damping ratio/% |
|---|---|---|---|
| LFO mode 1 | -0.0786±1.0623i | 0.1691 | 7.38 |
| LFO mode 2 | -0.0126±2.2178i | 0.3530 | 0.57 |
| LFO mode 3 | -0.0283±4.6020i | 0.7324 | 0.62 |

Table 6 shows the system's corresponding oscillation mode and its damping characteristics when the WT is located at ① in Fig (**3**) and the WT's capacity is 150MVA.

470

It can be seen from Table 6 that the system contains three low-frequency oscillation modes. In addition, in these modes, the damping ratio first drops and then rises as the frequency increases, but the overall trend is gradually decreasing.
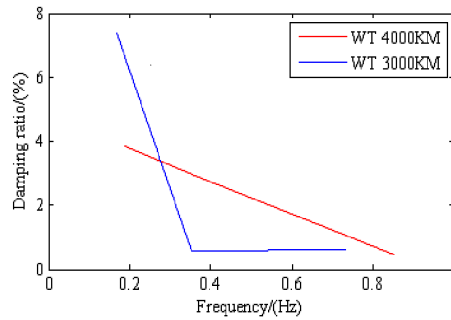


Fig. 7. Different transmission distance of DFIG-based WT in the rectifier side

As can be seen from the frequency-damping ratio characteristics in Fig. (**7**), when the WT is connected to system from the rectifier side of multi-terminal VSC-HVDC, at the same oscillation frequency, the greater the transmission distance of the WT, the greater the damping ratio.

Table 7: Oscillation model identification results

| Oscillation Mode | Eigenvalue | Frequency/Hz | Damping ratio/% |
|---|---|---|---|
| LFO mode 1 | -0.1327±1.3773i | 0.2192 | 9.59 |
| LFO mode 2 | -0.0103±5.0572i | 0.8049 | 0.20 |
| LFO mode 3 | -0.0757±5.4894i | 0.8737 | 1.38 |

Table 7 shows the system's corresponding oscillation mode and its damping characteristics when the WT is located at ② in Fig (**3**) and the WT's capacity is 150MVA. It can be seen from Table 7 that the rule is similar to Table 6's. At the same oscillation frequency, the greater the transmission distance of the WT, the greater the damping ratio when the WT is located at the Inverter side of multi-terminal VSC- HVDC system.
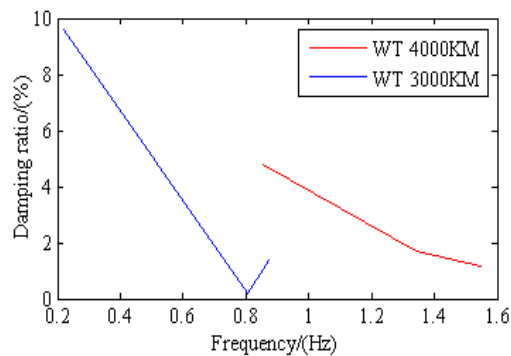


Fig. 8. Different transmission distance of DFIG-based WT in the Inverter side

As can be seen from the frequency-damping ratio characteristics in Fig. (**8**), when the WT is connected to the system from the multi-terminal VSC-HVDC inverter side, at the same low-frequency oscillation frequency, the greater the WT's transmission distance, the greater the damping ratio tends to be.

## 4. Conclusion

This paper establishes a model of the DFIG-based WT integrated into a three-terminal VSC-HVDC system. Through PSCAD/EMTDC platform simulation, the corresponding power angle curve is obtained and then the system is identified through the TLS-ESPRIT algorithm. At last, through eigenvalue analysis, the influence of different locations, different capacities, and different transmission distances of the WT connected to the three-terminal VSC-HVDC system on the oscillation mode and damping characteristics is studied. In addition, the specific conclusions are as follows:

(1) When the DFIG-based WT is connected to the three-terminal VSC-HVDC system from the rectifier side and the inverter side respectively, it will cause the system to produce corresponding low frequency oscillation modes, and its damping ratio will decrease with the increase of frequency. In addition, under the same oscillation frequency, the damping ratio when wind power is connected to the inverter side tends to be greater than that when it is connected to the rectifier side.

(2) Based on the different access points of the DFIG-based WT whether connected to the rectifier side or the inverter side of the VSC-HVDC system. When the WT's capacity increases from 100MVA to 150MVA, the damping ratio tends to increase as the capacity of the WT increases.

(3) Based on the different access points of the DFIG-based WT whether connected to the rectifier side or the inverter side of the VSC-HVDC system. When the transmission distance is reduced from 4000KM to 3000KM, as the transmission distance of WT increases, the damping ratio tends to increase.

## Acknowledgment

## References

[1] L. Michi et al., New HVDC technology in Pan-European power system planning, *2019 AEIT HVDC International Conference (AEIT HVDC)*, Florence, Italy, 1-6, 2019.
[2] N. U. Ahmad Chowdhury and A. Yanushkevich, Power flow analysis of meshed AC-DC super grid, *2015 IEEE Eindhoven PowerTech*, Eindhoven, 1-6, 2015.
[3] D. Fan, X. He, X. Gao and D. Wang, Analysis on submodule monitoring strategy of Nan'ao multi-terminal VSC-HVDC transmission system, *12th IET International Conference on AC and DC Power Transmission (ACDC 2016)*, Beijing, 1-4, 2016.
[4] D. Qiao et al., Analysis of Sub-synchronous Oscillation in the System Inteconnected with Offshore Wind farm by VSC-HVDC Based on Impedance Method, *2019 9th International Conference on Power and Energy Systems (ICPES)*, Perth, Australia, 1-5, 2019.
[5] H. Pang and X. Wei, Research on Key Technology and Equipment for Zhangbei 500kV DC Grid, *2018 International Power Electronics Conference (IPEC-Niigata 2018 -ECCE Asia)*, Niigata, 2343-2351, 2018.

[6]    G. Yang, W. Q. Wang, X. Aoran, G. Jing and C. L. Guo, Evaluation of Abandoned Wind Power by Neural Network Method, *2017 IEEE 7th Annual International Conference on CYBER Technology in Automation, Control, and Intelligent Systems (CYBER)*, Honolulu, HI, 543-546, 2017.

[7]    H. T. Cheng, J. X. Cheng, D. Yang, Y. Meng and P. Ge, Local Consumption Model of Wind and Photovoltaic Power Based on Demand Side Response, *2018 China International Conference on Electricity Distribution (CICED)*, Tianjin, 1933-1937, 2018.

[8]    R. Ye, F. Huang, Z. Lin, H. Wang and B. Wen, Influence of Power System Operation Mode on Wind Power Acceptance, *2017 4th International Conference on Information Science and Control Engineering (ICISCE)*, Changsha, 395-398, 2017.

[9]    H. Liu and J. Sun, Voltage Stability and Control of Offshore Wind Farms With AC Collection and HVDC Transmission, in *IEEE Journal of Emerging and Selected Topics in Power Electronics*, *2*(4), 1181-1189, 2014.

[10]   H. C. Liu, HVDC converters impedance modeling and system stability analysis[D]. Troy, NY: Rensselaer Polytechnic Institute, 2017．

[11]   J. Hu, H. Yuan and X. Yuan, Modeling of DFIG-Based WTs for Small-Signal Stability Analysis in DVC Timescale in Power Electronized Power Systems, in *IEEE Transactions on Energy Conversion*, *32*(3), 1151-1165, 2017.

[12]   L. Wang, C. Lin, H. Wu and A. V. Prokhorov, Stability Analysis of a Microgrid System With a Hybrid Offshore Wind and Ocean Energy Farm Fed to a Power Grid Through an HVDC Link, in *IEEE Transactions on Industry Applications*, *54*(3), 2012-2022, 2018.

[13]   Y. F. Wang, C. Y. Zhao, C. Y. Guo. Small signal stability and oscillation suppression method for islanded double fed induction generator-based wind farm integrated by modular multilevel converter based HVDC system[J]. *Transactions of China Electrotechnical Society*, 34(10), 2116-2129, 2019.

[14]   X. N. Xiao, C. L. Gu, et al. Analysis on damping characteristic of subsynchronous oscillation in AC /DC power grid consisting of 500 kV AC power transmission from Yimin to Fengtunand ± 500 kV DC power transmission from Hulunbuir to Liaoning[J]. *Power System Technology*, 35(10), 41-46, 2011.

[15]   Y. C. Choo, A. P. Agalgaonkar, K. M. Muttaqi, S. Perera and M. Negnevitsky, Subsynchronous torsional behaviour of a hydraulic turbine-generator unit connected to a HVDC system, *2008 Australasian Universities Power Engineering Conference*, Sydney, NSW, 1-6, 2008.

[16]   D. Xie, J. Q. Feng, Y. C. Lou, M. X. Yang, X. T. Wang, Small signal modeling and modal analysis of doubly-fed fan based on three-mass model[J], *Proceedings of the CSEE*, 33(S1), 21-29, 2013.

[17]   X. R. Xie, H. K. Liu, J. B. He, C. Y. Zhang, Y. Qiao, Analysis of the mechanism and characteristics of sub-synchronous oscillation caused by the interaction between direct drive wind farm and AC grid[J], *Proceedings of the CSEE*, *36*(09), 2366-2372, 2016.

[18]   S. H. Song, S. Q. Zhao, Analysis of the sub-synchronous oscillation of the doubly-fed wind farm through the flexible and direct grid-connected system based on the torque method[J], *Power System Technology*, *44*(02), 630-636, 2020.

[19]   B. Li et al., Study on the stability of large wind power grid-connected system including different types of wind generators, *2017 IEEE Conference on Energy Internet and Energy System Integration (EI2)*, Beijing, 1-6, 2017.

[20]   X. Kun, Z. W. Zhang, N. Wang and P. Zhang, Operation control and simulation research of the variable-speed constant-frequency system of the ship shaft generator, *2016 IEEE Region 10 Conference (TENCON)*, Singapore, 301-304, 2016.

[21]   R. Mahalakshmi, J. Viknesh and K. C. S. Thampatty, Mathematical modelling of grid connected Doubly Fed Induction Generator based wind farm, *2016 IEEE International Conference on Power Electronics, Drives and Energy Systems (PEDES)*, Trivandrum, 1-6, 2016.

[22]   T. Peng, L. Ze-Tao, H. Zheng-Hang, Z. Shi and H. Jun-Xian, Experimental Research on Grid-Connected Control System of DFIG with Uncertain Parameter, *2018 Chinese Automation Congress (CAC)*, Xi'an, China, 3350-3354, 2018.

[23]   J. Chen, T. Jin, M. A. Mohamed and M. Wang, An Adaptive TLS-ESPRIT Algorithm Based on an S-G Filter for Analysis of Low Frequency Oscillation in Wide Area Measurement Systems, in *IEEE Access*, *7*, 47644-47654, 2019.